ERA-40 Project Report Series no. 8

ECMWF ISLSCP-II near-surface dataset from ERA-40

A.K. Betts[1] and A.C.M. Beljaars

October 30, 2003

Research Department

Pittsford, VT 05763, USA , akbetts@aol.com

The Library
ECMWF
Shinfield Park
Reading, Berks RG2 9AX

library@ecmwf.int

Series: ECMWF ERA-40 Project Report Series

A full list of ECMWF Publications can be found on our web site under:
http://www.ecmwf.int/publications/

1. Introduction

This report summarizes the ECMWF (European Centre for Medium-range Weather Forecasts) near-surface data set for the second International Land-Surface Climatology Project (ISLSCP-II), which has been extracted for the years 1986-95 from the ECMWF '40-year' re-analysis (ERA-40, 1958-2002; Simmons and Gibson, 2000), which was extended to span 45 years: Sept. 1957- August, 2002. We discuss the components of the dataset, and show some comparisons with other ISLSCP datasets.

1.1 ERA-40 system

The purpose of ERA-40 was to produce an objective analysis of the atmosphere making optimal use of a wide range of observing systems. A recent version of the ECMWF Numerical Weather Prediction system (based on cycle 23r4) was used for the entire analysis period. The advantage of re-analysis over operational analysis is that no system changes occur that might affect the analysis products, although there are significant changes in the observations (see below). The primary reference for this reanalysis is http://www.ecmwf.int/research/era/. Links can be found for many aspects of ERA-40, including documentation of the cycle 23r4 Integrated Forecast System (IFS); and a summary and discussion of the observations available at different times during the 40-year reanalysis. The ERA-40 system has two main elements:

a) The analysis system that combined a background field in an optimal way with observations, and

b) A forecast model that provides the background field by propagating the atmospheric state from one time level to the next.

The ERA-40 system works intermittently with 6-hr intervals and uses observations between 3 hours before and after the analysis time to correct the background field. The forecasts run out to 9 hours to allow comparison with observations at the right time (First Guess at Appropriate Time, FGAT), but the increments are used at the analysis time corresponding to the 6 hour forecast. The analysis times are the standard meteorological observing times of 0, 6, 12, and 18 UTC.

The ECMWF forecast system is called the Integrated Forecasting System (IFS) and has been developed in co-operation with Meteo-France. For ERA-40 it is used with 60 levels, from the top of the model at 0.1 hPa to the lowest model level at about 10 m above the surface. The spectral resolution is T_L-159 (triangular truncation at wave number 159) with a corresponding resolution of about 125 km in grid point space. In grid point space, a so-called Reduced Gaussian grid is used which has 320 points around the world at the equator, but the number reduces at higher latitudes to obtain a nearly constant grid spacing at all latitudes. This reduced Gaussian grid is also used for the land surface parameters. The ISLSCP products have been interpolated from this grid to the 1x1 deg ISLSCP grid.

The analysis uses the so-called 3-dimensional variational method (3DVAR+FGAT), where a cost function in relation to observations and background is minimized. The weighting of the different parts of the cost function is controlled by estimates of observation errors and background errors. The spreading of observations in the horizontal and the vertical is controlled by horizontal and vertical correlation of the background errors. Most satellite observations (e.g. from TOVS instruments) are used by computing radiances from the model fields (forward model) and by comparing them with the satellite radiances. The analysis system uses a wide range of observations, from conventional radiosonde and SYNOP observations, to ocean winds from satellite scatterometry.

The analysis of T and q at the 2-m level and the snow depth analysis are part of the so-called "surface analysis" and use a successive correction method. The model first guess is used as a background field. Because large areas over land do not have snow depth observations, a weak relaxation is applied to a specified snow depth climatology. The increments in 2-m T and q are subsequently used in the soil moisture and soil temperature analysis using an optimal interpolation method (Douville et al., 2000).

The ISLSCP period of 1986-1995 spans changes in the satellite observations used in the analysis. The satellite microwave data from SSM/I was introduced in 1987 and the ERS data in 1991. The eruption of Pinatubo in 1991, which put volcanic aerosol into the stratosphere, impacts the TOVS radiances, which in turn impact the analysed tropical circulation and rainfall, mainly over the tropical oceans.

2. ISLSCP-II Parameters

2.1 Interpolation

ERA-40 spatial resolution is T_L-159. For ISLSCP-II, the data have been interpolated from the model reduced Gaussian grid (N80, described in http://www.ecmwf.int/products/data/technical/gaussian/) to the ISLSCP-II uniform 1 degree global grid, as much as possible consistent with the land-sea mask definitions. The ECMWF land sea mask (LSM) and the ISLSCP LSM are used to ensure that only land points are transformed into land points, and only sea points are used for sea points. For every grid point on the target grid, the 4 surrounding points of the input grid are considered, and only those points are selected that are of the same type as the target grid point (sea for sea and land for land). If all four points are of the same type, bi-linear interpolation is used. If the four neighbours do not all have the same type, the nearest neighbour of matching type is used. If all four neighbours have different type from the new point, they are all used. The latter applies to locations where for instance the ISLSCP LSM has a lake, whereas the ERA-40 LSM has land points in the surroundings only. In this case, the consistency between land sea masks is lost. Typically these are lakes in the middle of continents, where ERA-40 has no water point [such as Lake Tchad (13.5N, 13.5E) where the ISLSCP land-sea mask has 2 water points, whereas the ECMWF has only land points in the surrounding area], and small islands, where ERA has no land point at its T_L -159 resolution.

2.2 ISLSCP-II fields

The fields that are supplied for ISLSCP-II are near-surface meteorological fields (e.g. wind, humidity, temperature, pressure), fluxes (e.g. sensible and latent heat fluxes, radiative fluxes, stresses), and surface and sub-surface variables (e.g. sea surface temperatures, soil moisture, soil temperatures, snow variables). Some of these variables are constrained by observations (e.g. pressure, temperature, moisture); others are the result of parametrization (e.g. fluxes).

Data fields with their ECMWF identifiers are summarized in the Appendix.

There are 7 temporal resolutions in the data.

- Time invariant.
- Climatological monthly fields.
- Monthly means and 1st of month fields.
- Monthly averages of 6-hourly analysis fields and 3-hourly forecast fields.
- 6-hourly analysis fields
- 3-hourly forecast fields.

Some products are climatological fields that are constant during the period (but may have a specified annual cycle, such as background albedo). Some are only supplied as monthly averages, and on the first day of the month, such as the sub-surface variables over land. The land-surface scheme for ERA-40 and its parameters are discussed in Van den Hurk et al (2000).

Some products in this data set come with 3-hr time intervals, i.e. with higher frequency than the analysis cycle. The in-between fields are part of the first guess forecast, which is archived at forecast step 3 and 6. It is important to note that the difference between the 6 hour forecast and the analysis is always small; in other words the analysis increments are small. This means that for most applications it makes little difference whether short-range forecasts or analyses are used. We recommend using the 3 and 6-hour forecast fields, where 3-hourly time resolution is needed. A number of parameters do not even exist at analysis times, as they are computed by the forecast model. The fluxes are an example of the latter: these are accumulated from the start of each forecast. Precipitation with 3 hour time resolution is among the flux variables, but it suffers from spinup/spindown errors as discussed in section 3.2.

Exceptions are the 2-m temperature (T) and 2-m moisture (q) analyses. The 2-m level is not part of the model grid, and therefore it is not really part of the atmospheric analysis (although 2-m moisture observations are used for the analysis of moisture in the lowest model levels). A completely separate analysis of 2-m T and 2-m q is done and archived as analysis. This 2-m analysis is not used as initial condition for the next first guess; it is only used to support the soil moisture and soil temperature analysis (Douville et al., 2000). Parameters T and q at the 2-m level from forecasts are post-processing products and are obtained by interpolation between the lowest model level and the surface (consistent with the model parametrization using Monin-Obukhov similarity).

The data set includes several levels of information:

- Soil temperature and moisture for the four soil layers (0-7, 7-28, 27-100 and 100-289 cm depth).
- Snow depth, temperature and density.
- Surface fluxes of radiation, sensible and latent heat.
- “Top of the atmosphere” radiation fluxes.
- “Surface” atmospheric fields at 2-m and 10m (for wind).
- Atmospheric fields at the lowest model level 60 (about 10m above the surface).
- Atmospheric fields at model level 57 (about 100m above the surface).

3. Comparison of ERA-40 with selected ISLSCP-II products

The advantage of surface fields from model analyses is that they have complete coverage at 3-hourly time resolution. In contrast, surface observations are not uniformly distributed globally, and are sparse over many regions in the tropics, where only monthly mean data may be available, or even just climatology. Model products however have biases, related to the specific model. This near-surface dataset from ERA-40 is one of two in the ISLSCP-II dataset that have been derived from model analysis forecast systems (the other being that from NCEP). The NCEP and ECMWF analysis-forecast systems differ in their model structure, physical parameterization and horizontal and vertical resolution, and in their methods of processing the input observations. Consequently there are differences between the model surface fields. For the ERA-40, users should access http://www.ecmwf.int/research/era/ for updates on the known model biases as these become

available. Some discussion of the biases in surface fields over the Mississippi and Mackenzie basins is given in Betts et al. (2003a, b).

The ISLSCP data set contains also other near-surface products, some derived directly from surface observations, and some from satellite observations. In this section we show a few selected fields from ERA-40, and compare them with other datasets. We will show some mean differences from ISLSCP products from other sources, and some comparison anomaly fields.

3.1 Surface temperature and dewpoint fields.

Figure 1 (upper panels) shows winter (DJF: December, January, February) and summer (JJA: June, July and August) mean 2-m temperature from the ERA-40 surface analysis. There are nine winters in the DJF mean and ten summers in the JJA mean. The corresponding ERA-40 short-term forecast fields (not shown) are very similar. The very low JJA temperatures (below –55 C) over the Antarctic icecap do not appear with the contouring shown. The lower panels show the difference over land, ERA-40 - CRU, where CRU is the analysis interpolated directly from surface observations by the Climate Research Unit, Univ. of East Anglia, as archived for ISLSCP-II. ERA-40 tends to be a little cooler in the tropics than the CRU analysis, and a little warmer in high latitudes. Over regions of high terrain, ERA-40 is typically substantially warmer. There are differences in the orography used in the two analyses, and in mountainous regions data coverage is generally more limited, and is often in mountain valleys.

Figure 2 shows the corresponding plots for dewpoint (Td). The differences between the two analyses are generally small in regions of good data coverage, but become again larger in mountainous areas. There are some data voids in the CRU analysis.

Figures 3 and 4 compare the T and Td anomaly fields for two seasons: DJF1986 and JJA1987 for the two analyses. The anomaly fields for temperature (upper panels) are very similar, and do not show the differences between the mean analyses seen in Figure 1. The dewpoint anomalies for the most part are similar to the temperature anomalies. Over some data poor regions, such as Africa, there are larger differences between the analyses in their dewpoint anomalies than in their temperature anomalies.

3.2 Precipitation fields

The upper panels of Figure 5 show the broad similarity of the ERA-40 0-6-hr precipitation with the Global Precipitation Climatology Project (GPCP) analysis for the winter season, again as archived for ISLSCP. The left center panel shows the difference of ERA 0-6-hr precipitation from the CRU gauge precipitation analysis over land, and right center the corresponding difference from the GPCP analysis. Compared with the two analyses, ERA-40 has generally more precipitation in the tropics (see section 3.6.1), except over the Amazon, where it has a low bias, and less precipitation in the mid-latitudes. The lower panels show the corresponding difference from the ERA-40 24-36-hr FX. The model has a spin-up in the mid-latitude precipitation (in large-scale precipitation), which reduces the negative bias, and in some tropical regions a spin-down in precipitation, which reduces the positive bias.

Figure 6 shows the comparison for the northern summer JJA. The general tropical and mid-latitude biases and spinup/spindown characteristics are similar to Figure 5, and over Africa the ITCZ precipitation in ERA-40 does not extend as far north as in the analyses.

Figure 7 compares the ERA-40 and GPCP precipitation anomalies for DJF 1991 and JJA 1988. Despite the differences in their means, the anomaly patterns are remarkably similar, especially considering that the native GPCP analysis has a coarser horizontal resolution. This suggests that ERA-40 has a good representation of the circulation differences for these seasons.

3.3 Surface sensible and latent heat fluxes

The ERA-40 sensible heat flux (SH) for the northern winter and summer seasons is shown in Figure 8 (upper panels). We have no comparison for these from data, except the ocean climatology from 1945-1989 of Da Silva et al. (1994), so we shown the difference field from this climatology in the lower panels. Figure 9 shows the corresponding fields for the latent heat flux (LH) for the two seasons. There is a tendency for evaporation in ERA-40 over the oceans to be higher in mid-latitudes and lower in some regions of the tropics than the Da Silva climatology.

3.4 Surface radiation budget

Figures 10 to 16 compare the surface radiation budget of ERA-40 with the ISLSCP surface radiation budget (SRB) derived by Stackhouse et al (2000, 2003) from the ISCCP cloud data (Rossow and Schiffer, 1999). Figure 10 shows surface short-wave down (SWdown) for DJF and JJA from ERA-40 (upper panels) and the difference of ERA-40 from the corresponding SRB climatology (lower panels). ERA-40 has systematically less SWdown in the tropics and more in the mid-latitudes, suggesting that ERA-40 has generally more (optically thick) cloud in the tropics and less in the mid-latitudes than SRB. ERA-40 also has a high bias of SWdown in the stratocumulus regimes in the eastern oceans, where the model predicts too little cloud cover.

Figure 11 compares ERA-40 surface incoming (LWdown) and outgoing (LWup) radiation for the northern winter with the SRB data. There are major differences over the northern continents in winter. Both incoming and outgoing LW fluxes are larger in ERA-40. While this is consistent with the warm temperature bias of ERA-40 in winter at these latitudes (Figure 1), the difference in radiometric skin temperature implied by a 40 Wm^{-2} difference in LWup is of order 10K, much larger than the 2-m temperature bias of generally 1-3K seen in Fig. 1. The SRB LWup fluxes are low, because they use the NASA Data Assimilation Office 'GEOS-1' skin temperatures (Schubert et al. 1995), which have a cold bias in winter at high latitudes over land (Stackhouse et al. 2003). Over the Sahara, the pattern reverses, implying that ERA-40 has a cooler radiometric skin temperature.

Figure 12 is the corresponding figure for the northern summer, JJA. The lack of cloud over the ocean stratocumulus areas shows up as a deficit in the LWdown. ERA-40 LWdown is also lower than SRB over the Sahara and parts of central Asia; but higher over the Amazon and central Africa. The differences in LWup between the analyses are generally small over land, and tiny over the oceans, where both use similar sea surface temperature analyses.

Figure 13 shows ERA-SRB for SWnet and LWnet for DJF and JJA. In the tropics the patterns are similar for the two seasons, although the stratocumulus regimes are stronger during JJA. At high latitudes especially in the boreal winter, the LWnet in ERA-40 is much larger than SRB (which is near-zero at 60 ^{o}N over Canada and Russia: not shown). ERA-40 has generally a warm surface temperature bias (Fig. 1), but it is likely that the LW retrievals in SRB over high latitude land areas in winter are biased low (Stackhouse et al. 2003).

Figure 14 shows the ERA-40 surface all-sky albedo and the difference from the SRB albedo for northern Spring (MAM) and summer, JJA. We show spring, because the SRB SW fluxes are not retrievable in winter beyond 60 ^{o}N. ERA-40 has a prescribed seasonal cycle of background albedo, and computes a snow albedo using a tiled vegetation model (Van den Hurk et al. 2000). At high latitudes the winter albedo with snow in ERA-40 is less than that of the SRB analysis. Over many regions of the mid-latitudes ERA has a larger albedo than SRB. However, there are puzzling differences over the equatorial rain forests in Africa (which are not seen over the Amazon). The SRB albedo over the Congo is higher than ERA-40, and the difference increases significantly in JJA.

Figure 15 and 16 compare the anomalies in SWdown and LWdown for JJA1987 and DJF 1988. The anomaly patterns in SWdown are remarkably similar, while in the LW, the patterns are more similar in DJF 1988 than in JJA 1987. ERA-40 LWdown anomalies are generally smaller than those in SRB over the tropical oceans (not shown).

3.5 Discussion

These comparisons suggest that ERA-40 has a realistic representation of the seasonal anomaly fields on a global scale. A full set of the anomaly fields (from which the few shown here were selected) is available on request. However, in most cases, assessment of any mean biases in different products is more difficult, and will need further detailed work. The ERA-40 Report series can be consulted for updates (http://www.ecmwf.int/publications/library/do/references/list/192).

Many regional and local studies are also in progress. A series of papers, using river basin budgets for the Mississippi, Mackenzie, and Amazon basins are being written to assess the performance of ERA-40 over the Americas (Betts et al., 2003a, b). These evaluate surface fluxes and some other fields such as temperature. Improvements at high latitudes are discussed further in Betts et al. (2001). An evaluation of the diurnal cycle of precipitation and the surface thermodynamics over Amazonia is given in Betts and Jakob (2002a, b). Papers on earlier versions of the ECMWF model, include Betts et al. (1998, 1999); Betts and Viterbo (2000); and a comparison with an earlier NCEP reanalysis in Roads and Betts (2000).

3.6 Known problems with the ERA-40 products

3.6.1. Humidity analysis and rainfall over the tropical ocean

The most serious problem diagnosed in the ERA-40 analyses is the excessive tropical precipitation in later years particularly in production stream 1 after 1991.

Time series of total column water vapour (TCWV) averaged over the tropics show a change at the beginning of 1973, when humidity-sensitive radiances from the VTPR instrument are first assimilated and a more pronounced change with the introduction of TOVS/HIRS radiances from 1979. After this time, TCWV is generally higher and in reasonable agreement with independent retrievals from SMMR and SSM/I. In parallel, however, increments in TCWV become large and generally positive, with most of the added moisture rained out in the tropics in the six-hour forecasts. It shows as a clear correlation between the increment and precipitation. There is considerable interannual variability in these time series, but there is a general upward trend in the time series of increments and precipitation. Values from late 1991 to the end of 1997 lie above the general trend line, reflecting problems stemming from unmodelled effects of Pinatubo aerosol on HIRS radiances. The root cause of the trend appears, however, to lie elsewhere in the way the satellite data are assimilated. The general increase in increments and precipitation most likely reflects the increasing amount of satellite data assimilated, HIRS radiances from 1979 onwards, additional SSM/I data from one satellite in 1987 and data from two SSM/I satellites from 1999 onwards.

Compared with estimates from GPCP such as presented earlier, ERA-40 precipitation is substantially too large only in the tropics, especially over the oceans. Here patterns of precipitation appear realistic, but rainfall amounts in precipitating areas are much higher than GPCP values, and the discrepancy is larger than can be ascribed to uncertainties in the GPCP estimates (see Figs. 5, 6). ERA-40 precipitation is in much better agreement with GPCP in the extratropics, not only with respect to the climatological means but also with respect to the interannual variability of monthly totals.

Infrared VTPR and HIRS data are assimilated in ERA-40 only in regions judged to be cloud-free, and SSM/I data are assimilated only in regions judged to be rain-free. Background forecasts in these regions are drier than indicated by the data, and moistening increments result. The problem of excess rainfall appears to result from the way the humidity analysis spreads increments in the horizontal, which tends to add moisture in areas that are already close to saturation, in addition to adding it in the neighbouring areas that the data indicate are too dry. Rainfall is thus increased where it occurs naturally. There is the further possibility of an enhanced feedback via too-strong circulations and excess drying in descent regions driven by excessive latent-heat release, with associated increased moistening increments.

3.6.2. Arctic analyses since 1989

A further problem of concern is a cold bias in the lower troposphere (below about 500 hPa) over ice-covered oceans in both the Arctic and the Antarctic. A related problem in Arctic precipitation has also been identified. These polar cold biases arise from the assimilation of HIRS radiances. Changes to the thinning, channel-selection and quality control of the infrared data that were introduced for analyses from 1997 onwards (and for analyses prior to 1989) to reduce the tropical precipitation bias have also virtually eliminated the cold polar biases.

Although a new reanalysis will probably correct these issues in the future, it is not likely to be available for a few years.

3.6.3. Spinup of the hydrological cycle

The ERA-40 system has significant spinup at high latitudes of the precipitation field for 24-36 hours, associated with a problem in the moisture analysis (Betts et al., 2003b). The extent of this spinup can be assessed from the monthly mean precipitation fields which are given for four forecast intervals FX

FX : 0-6 hr (averaged over forecasts from 0, 6, 12, 18 UTC)

: 0-12 hr (averaged over forecasts from 0 and 12 UTC)

: 12-24 hr (averaged over forecasts from 0 and 12 UTC)

: 24-36 hr (averaged over forecasts from 0 and 12 UTC).

Betts et al. (2003a, b) discuss the spinup of precipitation over the Mississippi and Mackenzie River basins. Note that the 3-hrly fields and fluxes in the dataset, including precipitation, all come from the 0-6hr forecasts.

References

Betts, A. K., P. Viterbo and E. Wood, 1998: Surface energy and water balance for the Arkansas-Red river basin from the ECMWF reanalysis. *J. Climate*, **11**, 2881-2897.

Betts, A. K., J.H. Ball and P. Viterbo, 1999: Basin-scale surface water and energy budgets for the Mississippi from the ECMWF Reanalysis. *J. Geophys. Res.*, **104**, 19293-19306.

Betts, A. K. and P. Viterbo, 2000: Hydrological budgets and surface energy balance of seven subbasins of the Mackenzie River from the ECMWF model. *J. Hydrometeorol.*, **1**, 47-60.

Betts , A. K.,, P. Viterbo, A.C.M. Beljaars and B.J.J.M. van den Hurk,, 2001: Impact of BOREAS on the ECMWF Forecast Model. *J. Geophys. Res.*, **106,** 33593-33604.

Betts, A. K. and C. Jakob, 2002a, Evaluation of the diurnal cycle of precipitation, surface thermodynamics and surface fluxes in the ECMWF model using LBA data. *J. Geophys. Res.,* 107, 8045, doi:10.1029/2001JD000427.

Betts, A. K. and C. Jakob, 2002b, Study of diurnal cycle of convective precipitation over Amazonia using a single column model. *J. Geophys. Res.,* **107**, 4732, doi:10.1029/2002JD002264.

Betts, A. K., J. H. Ball, M, Bosilovich, P. Viterbo, Y. Zhang, and W. B.Rossow, 2003a. Intercomparison of Water and Energy Budgets for five Mississippi Sub-basins between ECMWF Reanalysis (ERA-40) and NASA-DAO fvGCM for 1990-1999. *J. Geophys. Res*., **108** (D16), 8618, doi:10.1029/2002JD003127. Also available in color as ERA-40 Project report series No. 7 from ECMWF, Reading RG2 9AX, UK, http://www.ecmwf.int/publications/library/ecpublications/_pdf/ERA40_PRS_7.pdf

Betts, A. K., J. H. Ball and P. Viterbo, 2003b: Water and energy budgets for the Mackenzie river basins from ERA-40. *J. Hydrometeorology*, in press. Also available in color as ERA-40 Project report series No. 6 from ECMWF, Reading RG2 9AX, UK,
http://www.ecmwf.int/publications/library/ecpublications/_pdf/ERA40_PRS_6.pdf

Da Silva, A., C.C. Young and S. Levitus, 1994: Atlas of surface marine data. Vol. 1: Algorithms and procedures. NOAA Atlas NESDIS 6. US Department of Commerce, Washington DC, 83pp.

Douville, H., P. Viterbo, J.-F. Mahfouf and A.C.M. Beljaars, Evaluation of optimal interpolation and nudging techniques for soil moisture analysis using FIFE data. *Mon. Wea. Rev., 128*, 1733-1756, 2000.

Roads, J. and A. K. Betts, 2000: NCEP/NCAR and ECMWF Reanalysis Surface Water and Energy Budgets for the GCIP Region. *J. Hydrometeorol.*, **1**, 88–94.

Rossow, W.B., and R.A. Schiffer, Advances in understanding clouds from ISCCP, *Bull. Amer. Meteorol. Soc., 80*, 2261-2287, 1999.

Schubert, S., C.-K. Park, C.-Y. Wu, W. Higgins, Y. Kondratyeva, A. Molod, L. Takacs, M. Seablom, R. Rood, 1995: A multiyear assimilation with the GEOS-1 system: Overview and results. NASA Tech. Memo. No. 104606, volume 6, Goddard Space Flight Center, Greenbelt, MD 20771. Available online from http://dao.gsfc.nasa.gov/subpages/tech-reports.html.

Simmons A.J. and J.K. Gibson, 2000. The ERA-40 Project Plan, ERA-40 Project Report Series No. 1, ECMWF, Reading RG2 9AX, UK., 63pp.

Stackhouse, P. W., S. K. Gupta, S. J. Cox, M. Chiacchio, and J. C. Mikovitz, 2000: The WCRP/GEWEX. Surface Radiation Budget Project Release 2: An assessment of surface fluxes at 1 degree resolution. In *IRS 2000: Current Problems in Atmospheric Radiation,* W. L. Smith and Y. M. Timofeyev, Eds*., International Radiation Symposium,* St. Petersburg, Russia, July 24-29, 2000.

Stackhouse, P.W., Jr., S. J. Cox, S. K. Gupta, J.C. Mikovitz, M. Chiacchio, 2003: The WCRP/GEWEX Surface Radiation Budget Data Set: A 1 degree resolution, 12 year flux climatology. (in preparation)

Van den Hurk, B.J.J.M., P. Viterbo, A.C.M. Beljaars and A. K. Betts, 2000: Offline validation of the ERA-40 surface scheme. *ECMWF Tech Memo, 295*, 43 pp., Eur. Cent. For Medium-Range Weather Forecasts, Shinfield Park, Reading RG2 9AX, England, UK.

Acknowledgments

Alan Betts acknowledges support from NSF under Grant ATM-9988618, and from the NASA Land-surface Hydrology Program under Grant NAS5-11578, which also supported the production of this dataset at ECMWF. Data extraction and interpolation to the ISLSCP grid was done by Keith Fielding (ECMWF data services). The authors would like to thank the ERA-40 team at ECMWF and in particular Adrian Simmons and Sakari Uppala for careful reading of an early version of this report.

Appendix 1. Description of the ERA-40 ISLSCP-II fields

The fields as supplied to the ISLSCP project were put in different files according to their type. This Appendix describes the data structure of the fields as supplied by ECMWF to the ISLSCP Project Office at NASA Goddard, so that fields can be traced back to their grib identifiers in the ECMWF archive. In the ISLSCP archive, the instantaneous parameters are unchanged. However, the flux parameters, which are accumulated fields in the ECMWF archive, were divided by the time interval (3* 3600 or 6*3600s) to change them to fluxes in the ISLSCP archive.

A file may contain a large number of fields which are identified by:

PARAM = grib code that identifies the parameter (see subsections).

DATE = date representing the start of a forecast or analysis time.

TIME = time representing the start of a forecast or analysis time.

STEP = forecast step in hours (0 for analysis).

STREAM = 1025 for daily archive, i.e. normal analyses and forecasts,
1043 for monthly means at SYNOP times
1070 for monthly s.d. at SYNOP times
1071 for monthly daily averages
1072 for monthly s.d. over different times of the day

Two types of parameters exist:

(i) Instantaneous parameters, and

(ii) time integrated (accumulated) parameters.

Model variables (e.g. wind, temperature, moisture, soil temperature) are instantaneous parameters.

All fluxes are integrated since the start of the forecast (e.g. precipitation, turbulent fluxes, radiative fluxes). This can be seen from the listed units (e.g. the total precipitation in the time interval has units of meters). For instance the 3 hour forecast is an integral over 3 hours (3*3600 sec) and the 6 hour forecast over 6 hours, so in order to get the average from 3 to 6 it is necessary to subtract the two fields and to divide by the time interval of 3*3600s. This has been done in the ISLSCP data base. Note that this can produce some very small, spurious values, related to the limited accuracy of the GRIB packing in the original archive. The GRIB packing takes the minimum and maximum of a field and divides the range between min and max in 2**16 levels. The max and min are different for the 3 and 6 hour forecasts, so for example it is possible that the accumulation for 6 hours has a smaller number than the accumulation for 3, giving on subtraction a spurious small negative value. The user will notice this for fields like precipitation, because it has some points with very high values in the Tropics.

A.1 Fixed fields

These fields are so called climatological fields and are constant during the project. The background albedo is a monthly field that is interpolated in time between the 15th of each month in order to obtain a smooth seasonal evolution.

GRIB CODE	GRIB ID	Description	units
173	SR	Surface roughness length for momentum	(m)
234	LSRH	Logarithm of surface roughness length for heat	(-)
174	AL	Albedo background (monthly)	(0-1)
129	Z	Geopotential of model surface (Orography * g)	(m2/s2)
172	LSM	Land-sea mask (> 0.5 means land)	(0-1)
027	CVL	Low vegetation fraction	(0-1)
028	CVH	High vegetation fraction	(0-1)
029	TVL	Low vegetation dominant type	(-)
030	TVH	High vegetation dominant type	(-)

The land-surface scheme in ERA-40 has separate tiles for high (that is forests) and low vegetation classes, that are treated using different physical paramererizations (Van den Hurk et al., 2000). [For example, at high latitudes, there is a tile for “high vegetation with snow beneath”, which has a distinct energy budget for the snow layer, that is only partly coupled to the boundary layer. In addition, snow beneath forests has a much lower albedo (15%) to represent the shading effect of the canopy, than snow lying on top of low vegetation (whether tundra, marsh or cropland)]. In ERA-40, each grid square has a vegetation fraction and one (dominant) vegetation type for both high and low vegetation.

A.2 Monthly averages + 1st of the month + st. dev. (Analyses)

Monthly averages: step : 0; stream : 1071
1st of the month: step : 0; stream : 1025
Standard deviations: step : 0; stream : 1072

Averages have been obtained by averaging over analyses for 0, 6, 12, 18 UTC and all days of the month (Grib headers DD=0)

- 1st of the month is for the analyses of 12 UTC
- St. Devs. have been obtained from fields of 0, 6, 12, 18 UTC and all days of the month

GRIB CODE	GRIB ID	Description	units
141	SD	Snow depth	(m of water)
032	ASN	Snow albedo	(0-1)
033	RSN	Snow density	(kg/m3)
238	TSN	Snow temperature	(K)
039	SWVL1	Soil moisture layer 1	(m3/m3)
040	SWVL2	Soil moisture layer 2	(m3/m3)
041	SWVL3	Soil moisture layer 3	(m3/m3)
042	SWVL4	Soil moisture layer 4	(m3/m3)
139	STL1	Soil temperature layer 1 over land [and SST over ocean]	(K)
170	STL2	Soil temperature layer 2	(K)
183	STL3	Soil temperature layer 3	(K)
236	STL4	Soil temperature layer 4	(K)
031	CI	Sea ice fraction	(-)
022	*	Soil moisture availability index(root zone)	(0-1)
023	*	Soil moisture availability index(bare soil)	(0-1)

[fields 022 and 023 are derived variables and do not have a GRIB ID]
[fields 022, 023 and 031 do not have a standard deviation]

A.3 Monthly averages of precipitation (forecasts)

step : 0-6 (averaged over forecasts from 0,6,12, 18 UTC)
: 0-12 (averaged over forecasts from 0,12 UTC)
: 12-24 (averaged over forecasts from 0,12 UTC)
: 24-36 (averaged over forecasts from 0,12 UTC)
stream : 1071

```
142   LSP     Precipitation large scale                  (m/day of water)
143   CP      Precipitation convective                   (m/day of water)
144   SF      Snow fall                                  (m/day of water)
```

In the model precipitation is represented by 4 terms: large-scale rain, convective rain ; large-scale snowfall and convective snowfall.

LSP is the sum of terms 1 + 3
CP is the sum of terms 2 + 4
SF is the sum of terms 3 + 4
so total precipitation is the sum of LSP+CP.

These are monthly averages from short-term forecasts. The model analysis cycle uses 6-hour forecasts from analyses at 00, 06, 12, and 18 UTC. From the 00 and 12 UTC analyses, forecasts were extended to 36 hours. The first monthly average is summed from the four 6-hourly segments of the analysis cycle. Three additional monthly averages are constructed by summing twice-daily segments of the 0-12, 12-24, 24-36 hour forecasts, all verifying at the same time. These four different precipitation averages are included, because precipitation has a significant spinup in the first 36 hours. A discussion of the spinup of ERA-40 precipitation is given in Betts et al. (2003a, b).

A.4 Monthly averages of 6 hourly fields (analyses)

time : 0,6,12,18
step : 0
stream : 1043

167	2T	Temperature at 2m level	(K)
168	2D	Dew point at 2m level	(K)
165	10U	U-component of wind speed at 10 m	(m/s)
166	10V	V-component of wind speed at 10 m	(m/s)
207	10SI	Horizontal wind speed at 10 m	(m/s)
131	U57	U-component of wind speed at level 57	(m/s)
132	V57	V-component of wind speed at level 57	(m/s)
130	T57	Temperature at level 57	(K)
133	q57	Specific humidity at level 57	(kg/kg)
131	U60	U-component of wind speed at level 60	(m/s)
132	V60	V-component of wind speed at level 60	(m/s)
130	T60	Temperature at level 60	(K)
133	q60	Specific humidity at level 60	(kg/kg)
152	LNSP	Logarithm of surface pressure in(Pa)	

Monthly standard deviation of analyses for different synoptic times:

filename: mo_sd_an_4.4_YYYY
time : 0,6,12,18
step : 0
stream : 1070

167	2T	Temperature at 2m level	(K)
168	2D	Dew point at 2m level	(K)
165	10U	U-component of wind speed at 10 m	(m/s)
166	10V	V-component of wind speed at 10 m	(m/s)
131	U57	U-component of wind speed at level 57	(m/s)
132	V57	V-component of wind speed at level 57	(m/s)
130	T57	Temperature at level 57	(K)
133	q57	Specific humidity at level 57	(kg/kg)
131	U60	U-component of wind speed at level 60	(m/s)
132	V60	V-component of wind speed at level 60	(m/s)
130	T60	Temperature at level 60	(K)
133	q60	Specific humidity at level 60	(kg/kg)

A.5 Monthly averages of 3 hourly fields (forecasts)

Monthly averaged forecasts for different synoptic times:

time : 0,6,12,18

step : 3,6

stream : 1043

Monthly standard deviations of forecasts for different synoptic times:

time : 0,6,12,18

step : 6

stream : 1070

-Monthly averages have been obtained separately for different times of the day.

167	2T	Temperature at 2m level	(K)
168	2D	Dew point at 2m level	(K)
165	10U	U-component of wind speed at 10 m	(m/s)
166	10V	V-component of wind speed at 10 m	(m/s)
207	10SI	Horizontal wind speed at 10 m	(m/s)
152	LNSP	Logarithm of surface pressure in (Pa)	
180	EWSS	U stress	(Ns/m2)
181	NSSS	V stress	(Ns/m2
176	SSR	Surface net SW rad	(Ws/m2)
177	STR	Surface net LW rad	(Ws/m2)
169	SSRD	Surface SW downward	(Ws/m2)
175	STRD	Surface LW downward	(Ws/m2)
178	TSR	TOA net SW rad	(Ws/m2)
179	TTR	TOA net LW rad	(Ws/m2)
146	SSHF	Surface SH flux	(Ws/m2)
147	SLHF	Surface LH flux	(Ws/m2)
182	E	Surface evaporation	(m of water)
044	ES	Snow evaporation	(m of water)
045	SMLT	Snow melt	(m of water)
142	LSP	Precipitation large scale	(m of water)
143	CP	Precipitation convective	(m of water)
144	SF	Snow fall	(m of water)
205	RO	Runoff	(m of water)

[field 152 is only available at step 6]
[fields 152 and 207 do not have standard deviation]

The standard deviations have the same units as the corresponding fields. The consequence for time integrated fluxes is that the standard deviations of time integrated fluxes have to be divided by the accumulation time interval. For example, the standard deviation of SSHF for time=12, step=6, is obtained by dividing by 6*3600 and refers to the standard deviation of the averaged flux between 12 and 18 UTC.

A.6 6-hourly fields (analyses)

time : 0,6,12,18
step : 0
stream : 1025

167	2T	Temperature at 2m level	(K)
168	2D	Dew point at 2m level	(K)

A.7 3-hourly fields (forecasts)

time : 0,6,12,18
step : 3,6
stream : 1025

167	2T	Temperature at 2m level	(K)
168	2D	Dew point at 2m level	(K)
165	10U	U-component of wind speed at 10 m	(m/s)
166	10V	V-component of wind speed at 10 m	(m/s)
131	U57	U-component of wind speed at level 57	(m/s)
132	V57	V-component of wind speed at level 57	(m/s)
130	T57	Temperature at level 57	(K)
133	q57	Specific humidity at level 57	(kg/kg)
131	U60	U-component of wind speed at level 60	(m/s)
132	V60	V-component of wind speed at level 60	(m/s)
130	T60	Temperature at level 60	(K)
133	q60	Specific humidity at level 60	(kg/kg)
152	LNSP	Logarithm of surface pressure in (Pa)	
235	SKT	Skin temperature	(K)
180	EWSS	U stress	(Ns/m2)
181	NSSS	V stress	(Ns/m2
176	SSR	Surface net SW rad	(Ws/m2)
177	STR	Surface net LW rad	(Ws/m2)
169	SSRD	Surface SW downward	(Ws/m2)
175	STRD	Surface LW downward	(Ws/m2)
146	SSHF	Surface SH flux	(Ws/m2)
147	SLHF	Surface LH flux	(Ws/m2)
182	E	Surface evaporation	(m of water)
142	LSP	Precipitation large scale	(m of water)
143	CP	Precipitation convective	(m of water)
144	SF	Snowfall	(m of water)
205	RO	Runoff	(m of water)

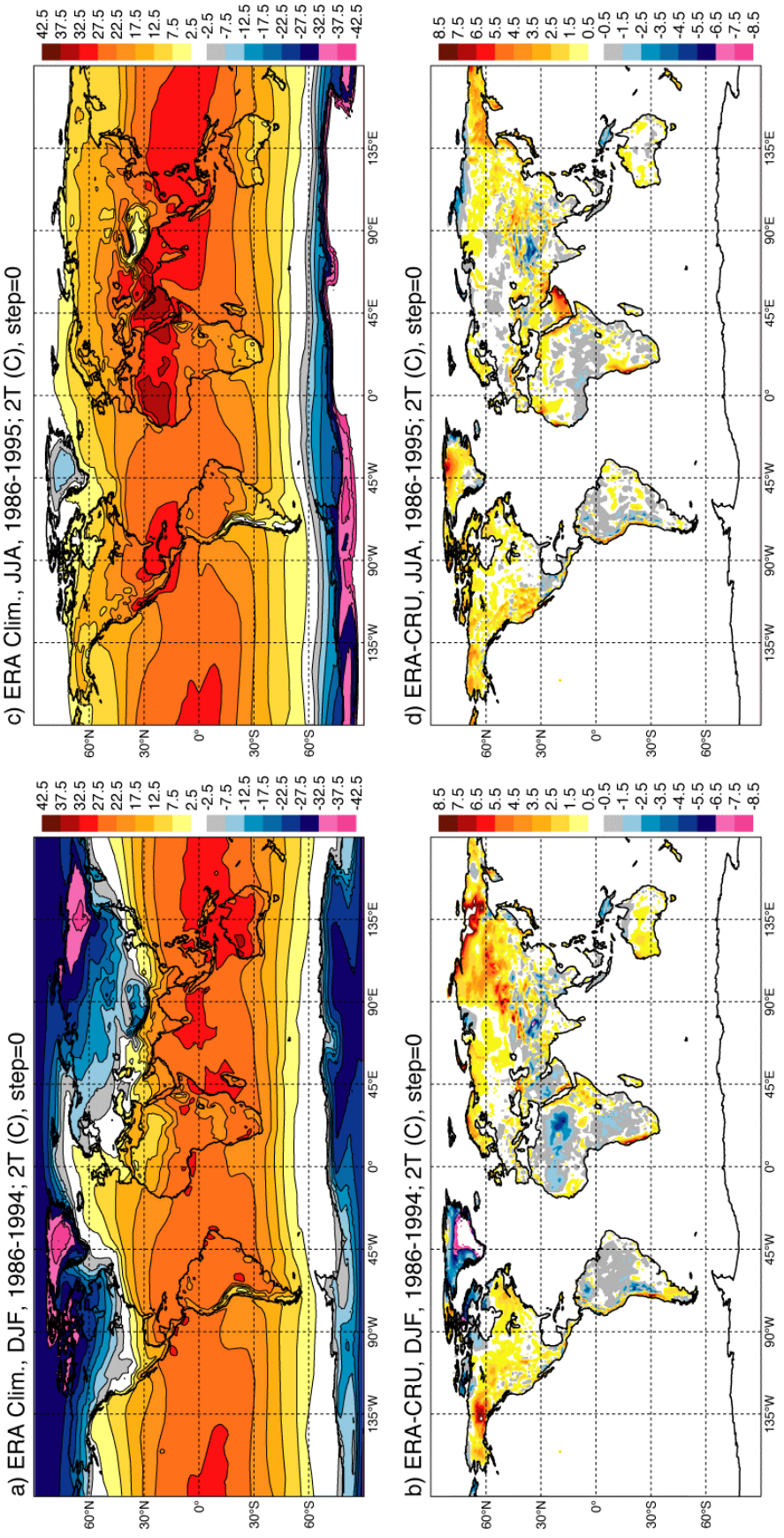

Figure 1. Winter (DJF: December, January, February) and summer (JJA: June, July and August) ERA-40 2-m temperature and differences from CRU.

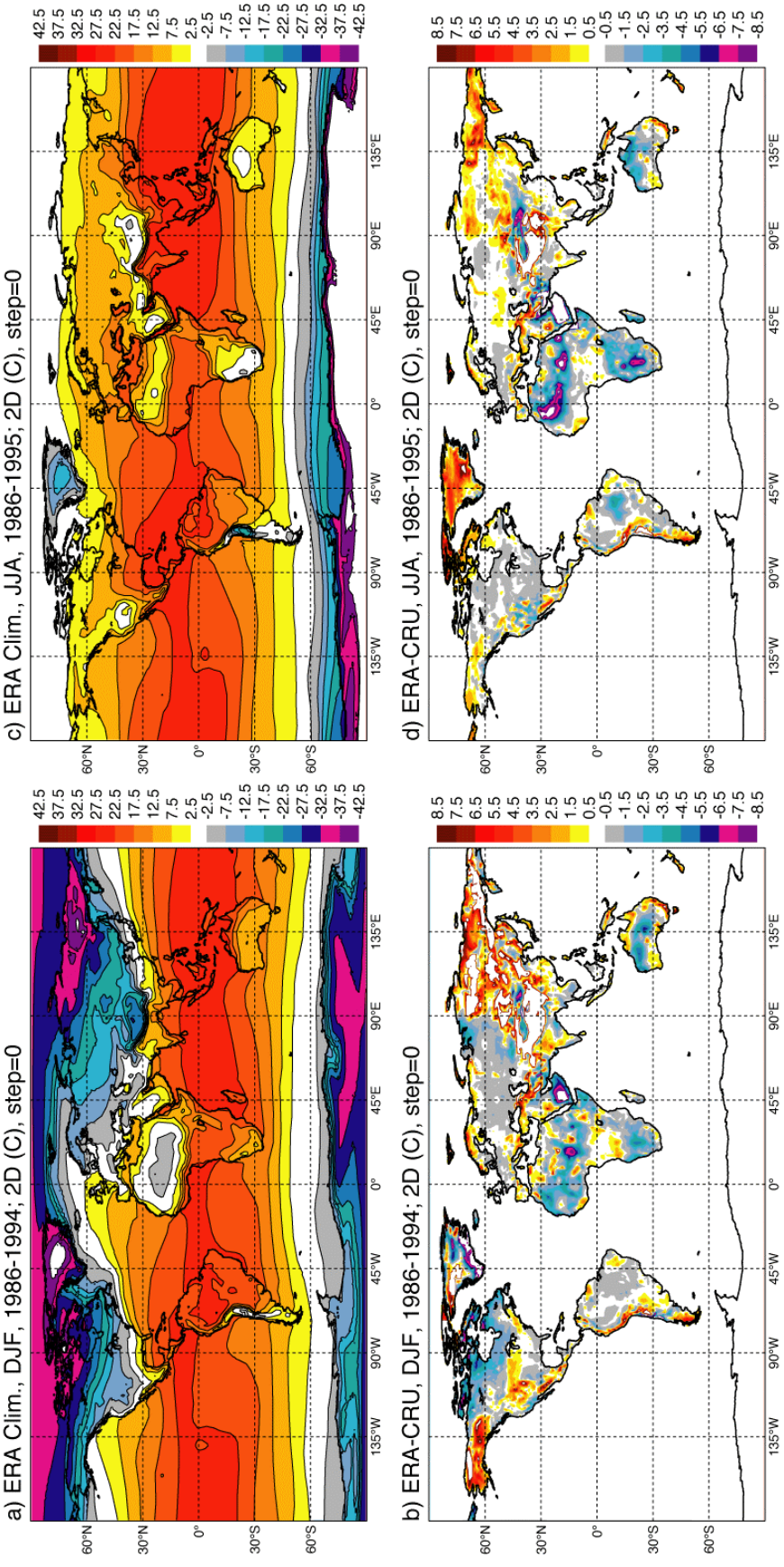

Figure 2. As Figure 1 for 2-m dewpoint.

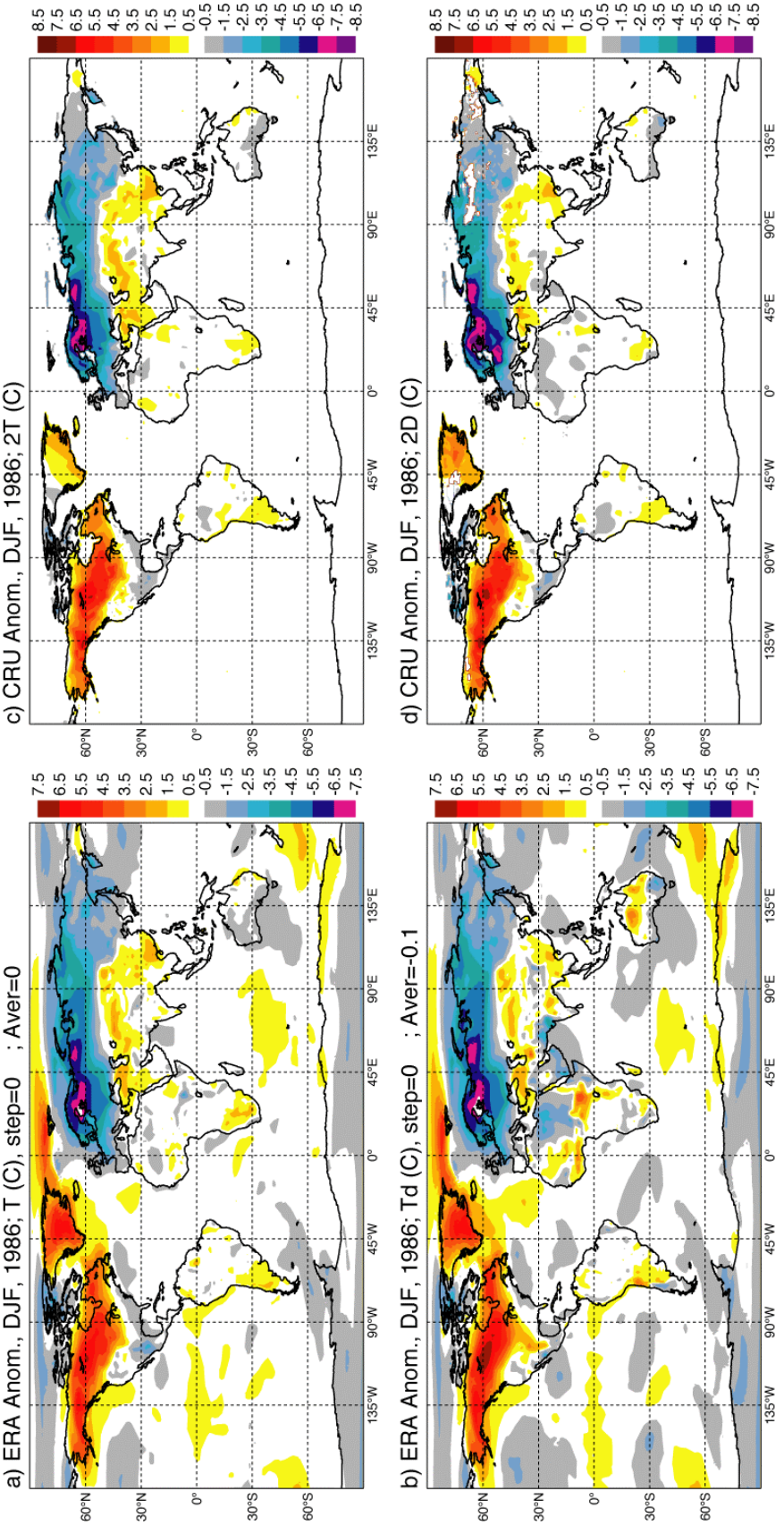

Figure 3: Anomaly fields for T (upper panels) and Td (lower panels) for DJF1986 from ERA-40 and CRU analyses.

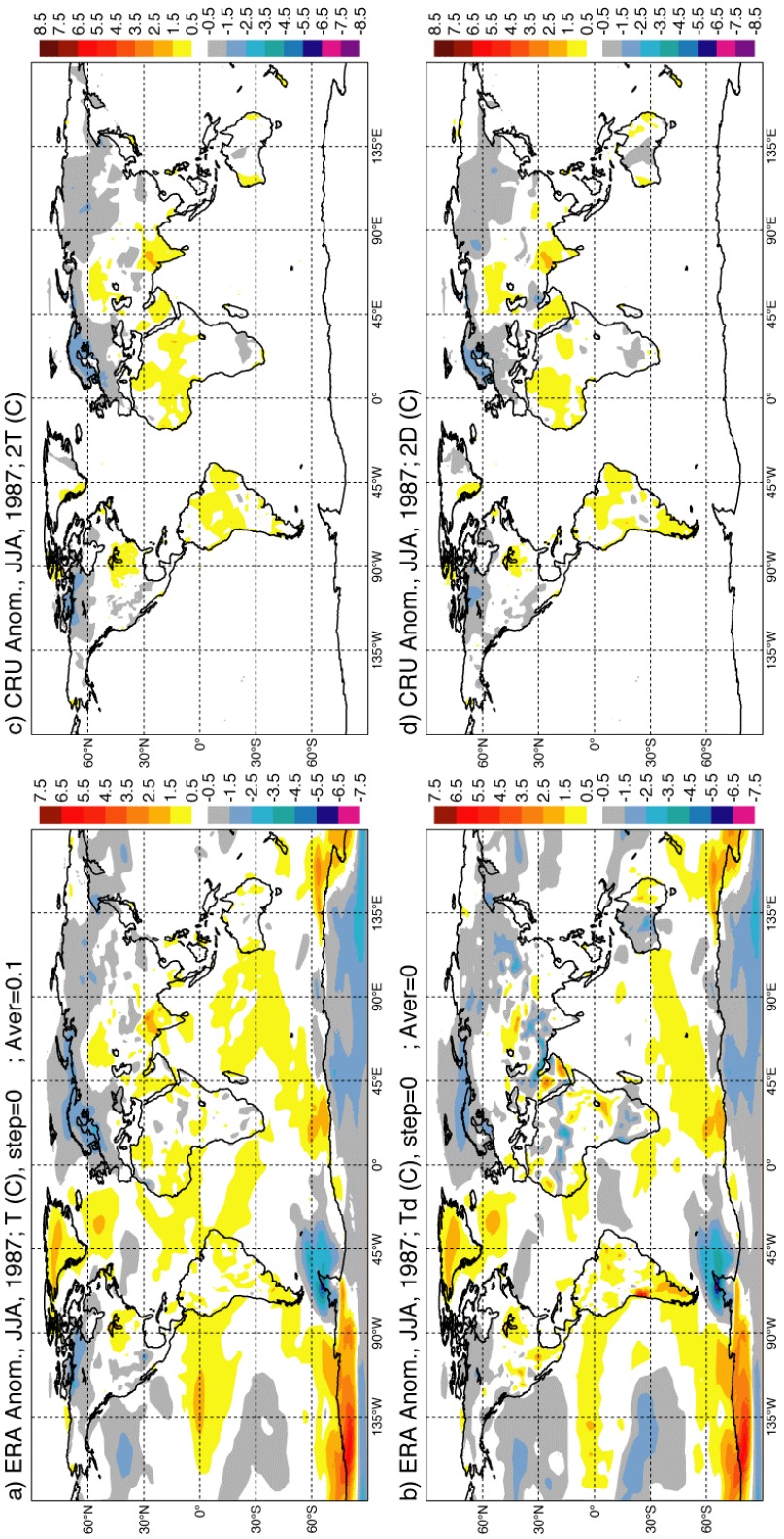

Figure 4: As Figure 3 for JJA1987.

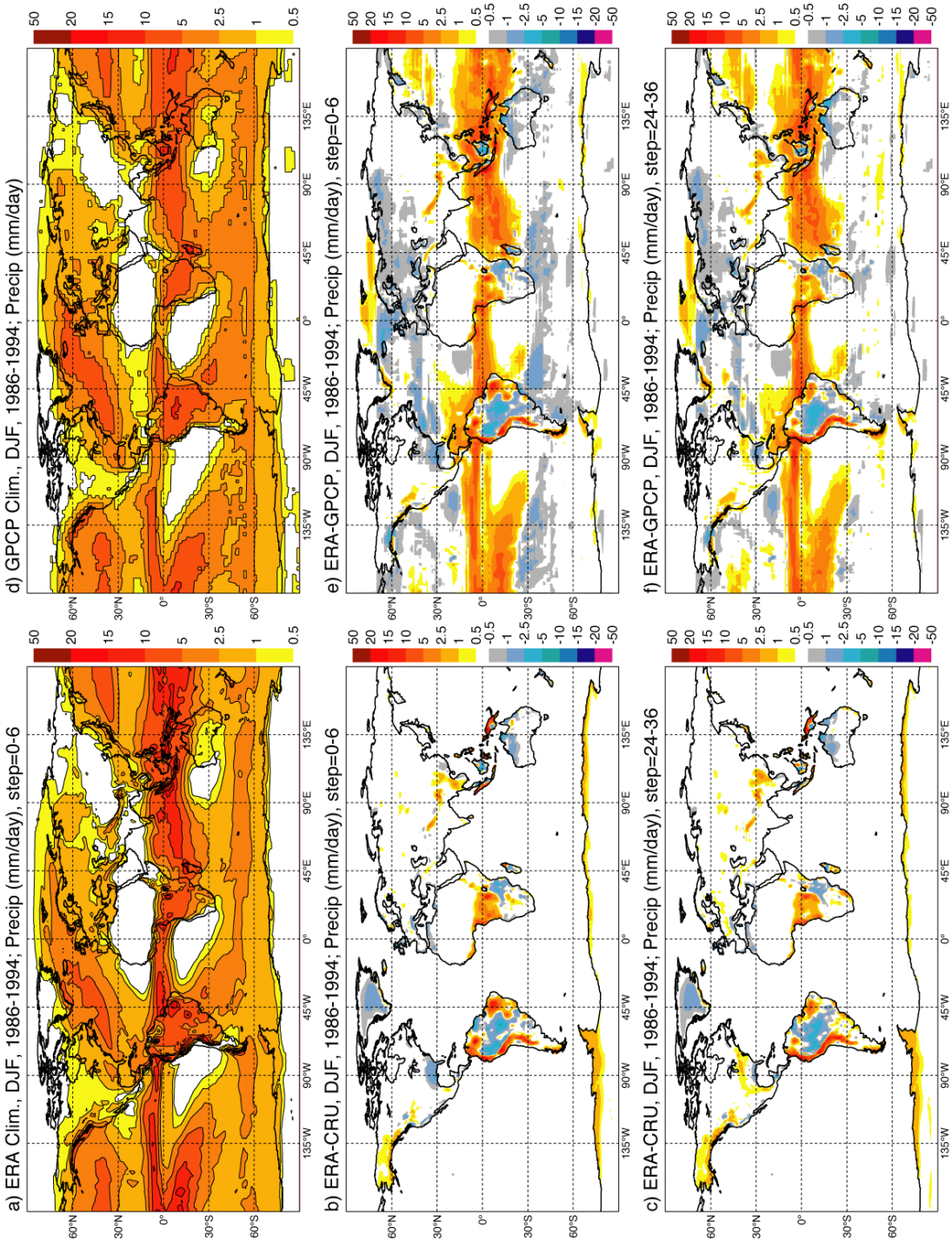

Figure 5: Comparison of ERA-40 0-6-hr precipitation with the GPCP analysis for the winter season (upper panels); difference of ERA 0-6-hr precipitation from the CRU gauge precipitation analysis over land (centre left), and from the GPCP analysis (centre right). The lower panels show the corresponding differences from the ERA-40 24-36-hr forecasts.

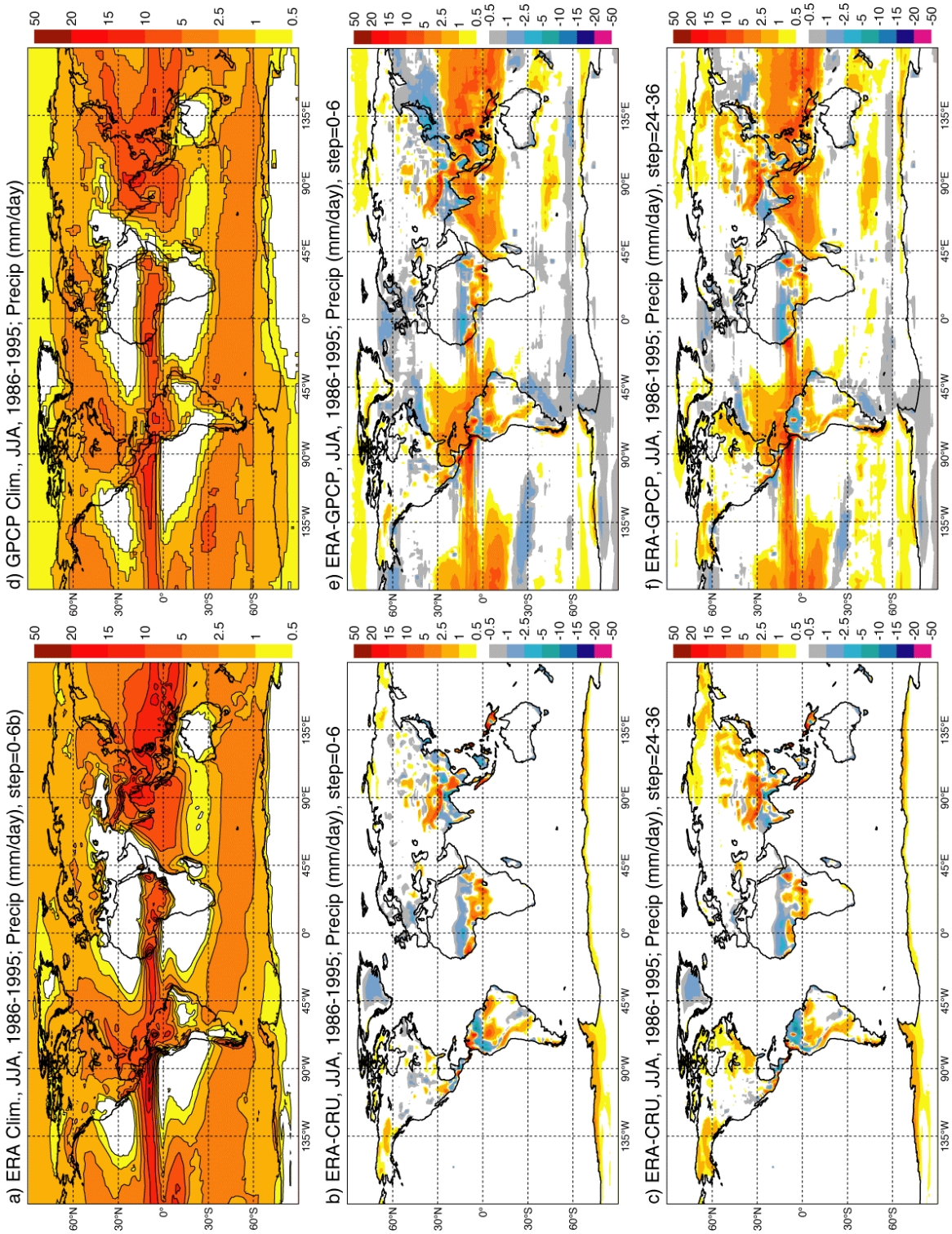

Figure 6: As Figure 5 for the northern summer.

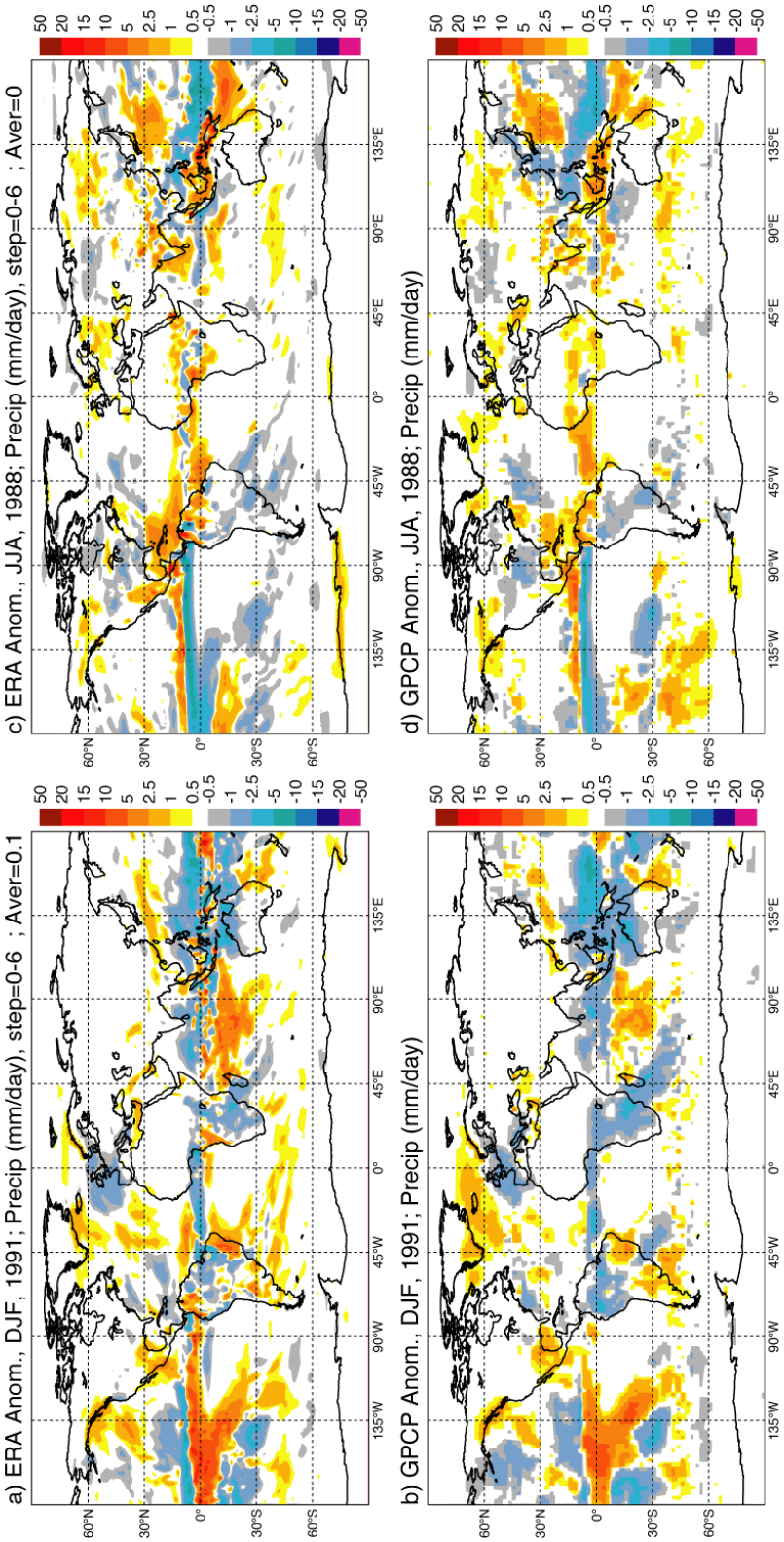

Figure 7: Comparison of ERA-40 and GPCP precipitation anomalies for DJF 1991 and JJA 1988.

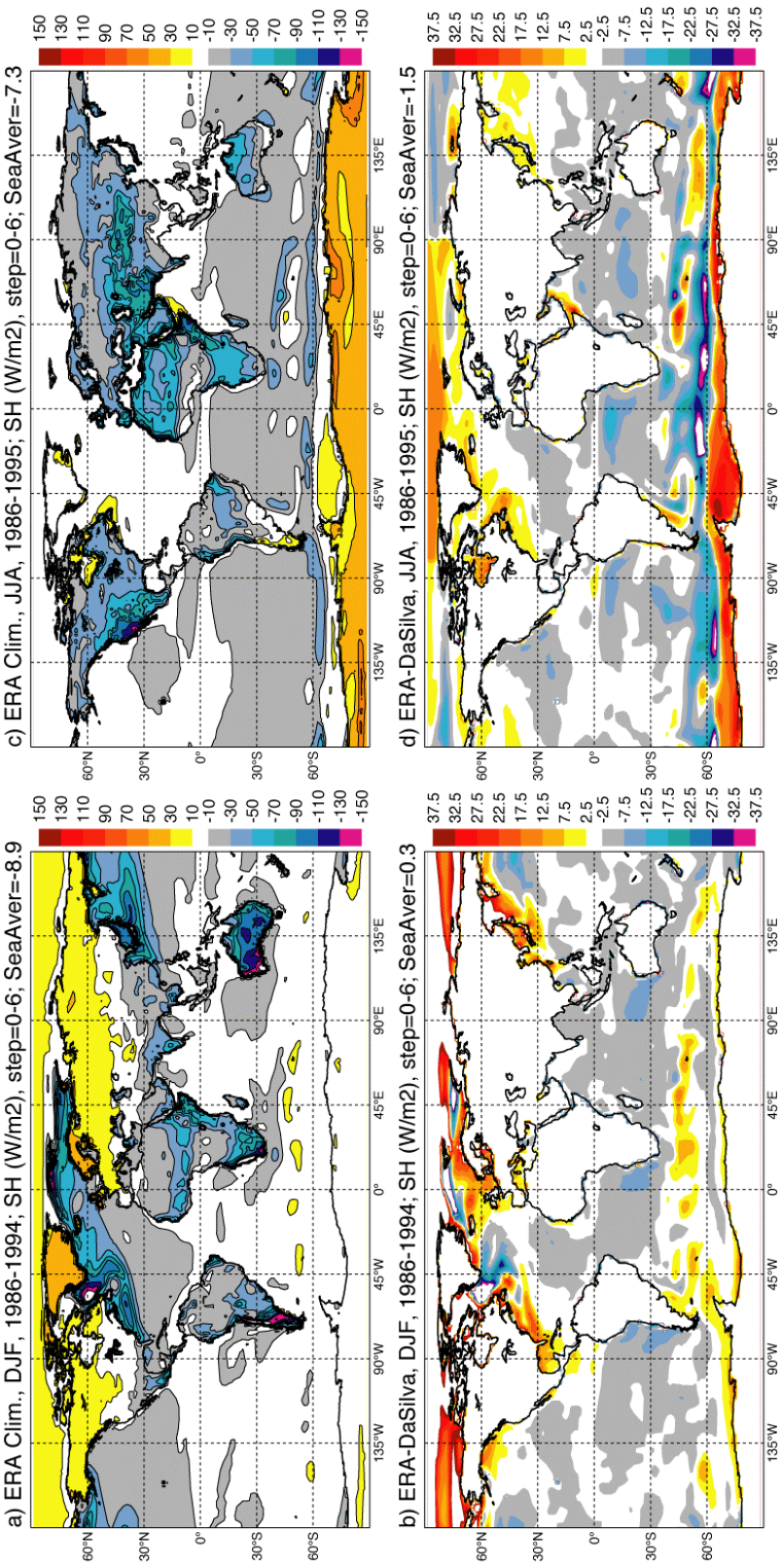

Figure 8: ERA-40 sensible heat flux (SH) for the northern winter and summer seasons (upper panels); and difference from the ocean climatology of da Silva et al. (lower panels).

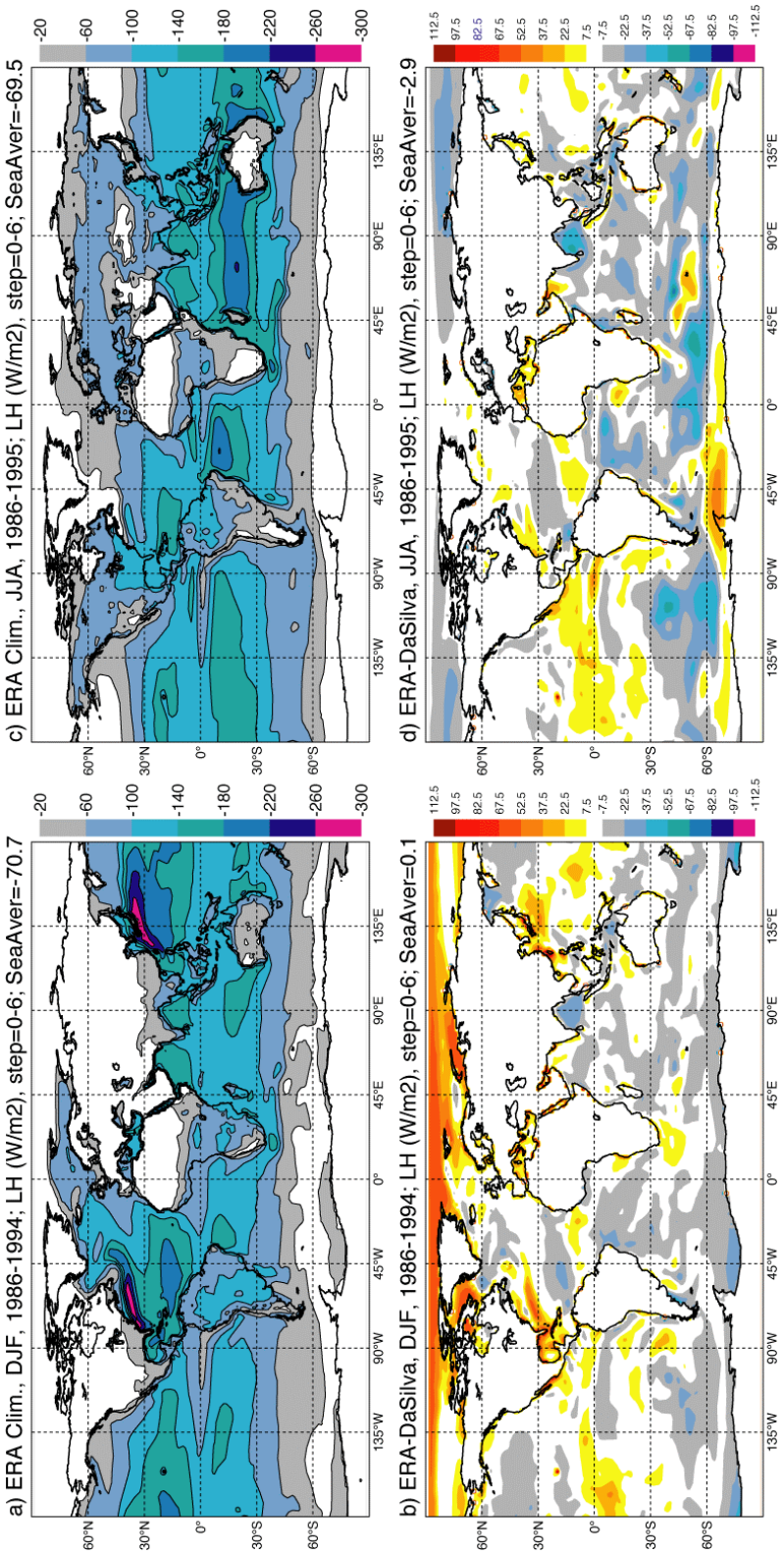

Figure 9: As Figure 8 for latent heat flux (LH).

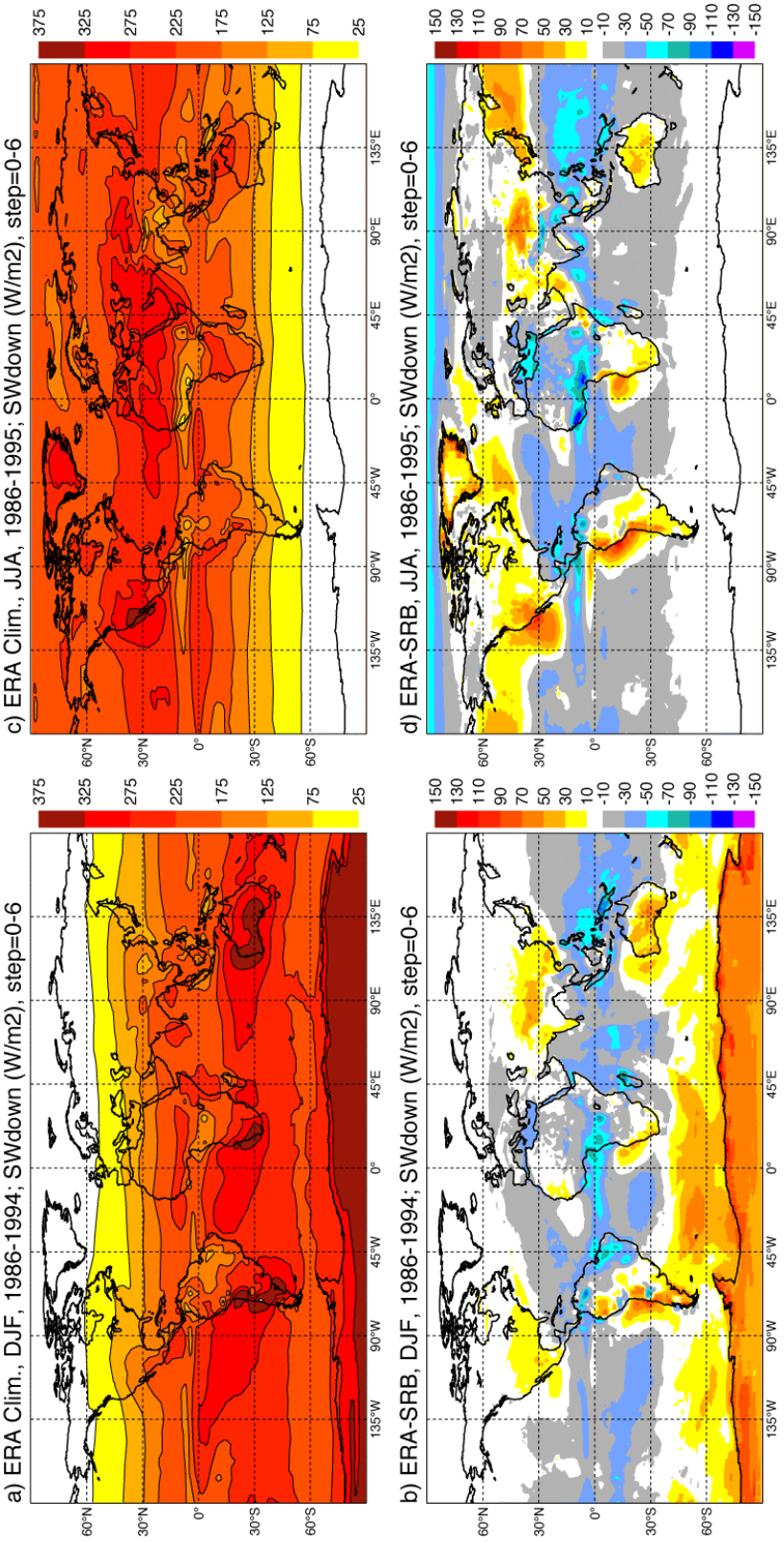

Figure 10: Surface short-wave down (SWdown) for DJF and JJA from ERA-40 (upper panels); difference of ERA-40 from the corresponding SRB climatology (lower panels).

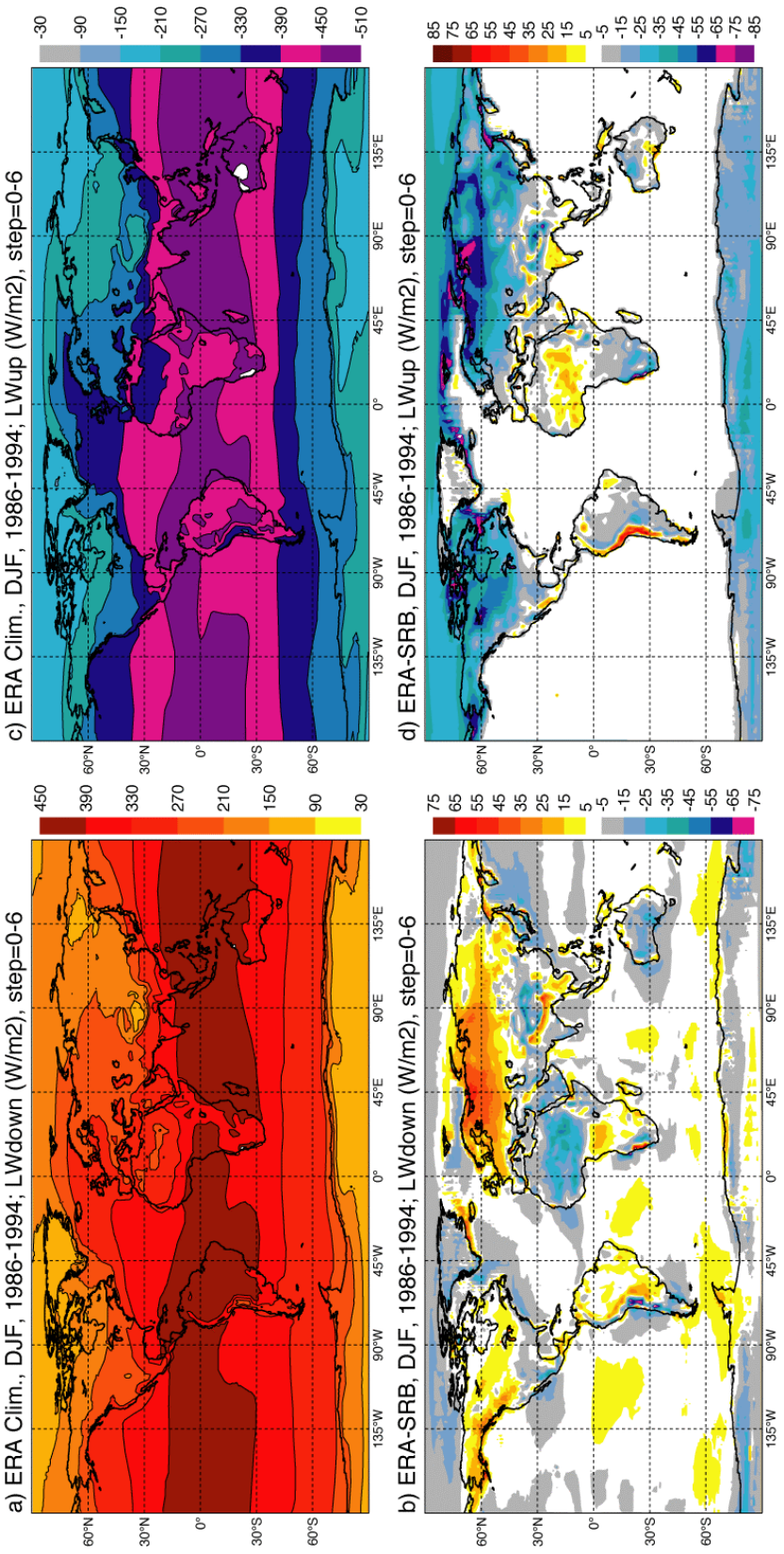

Figure 11: ERA-40 surface incoming (LWdown) and outgoing (LWup) radiation for the northern winter, DJF (upper panels) and difference from SRB data (lower panels).

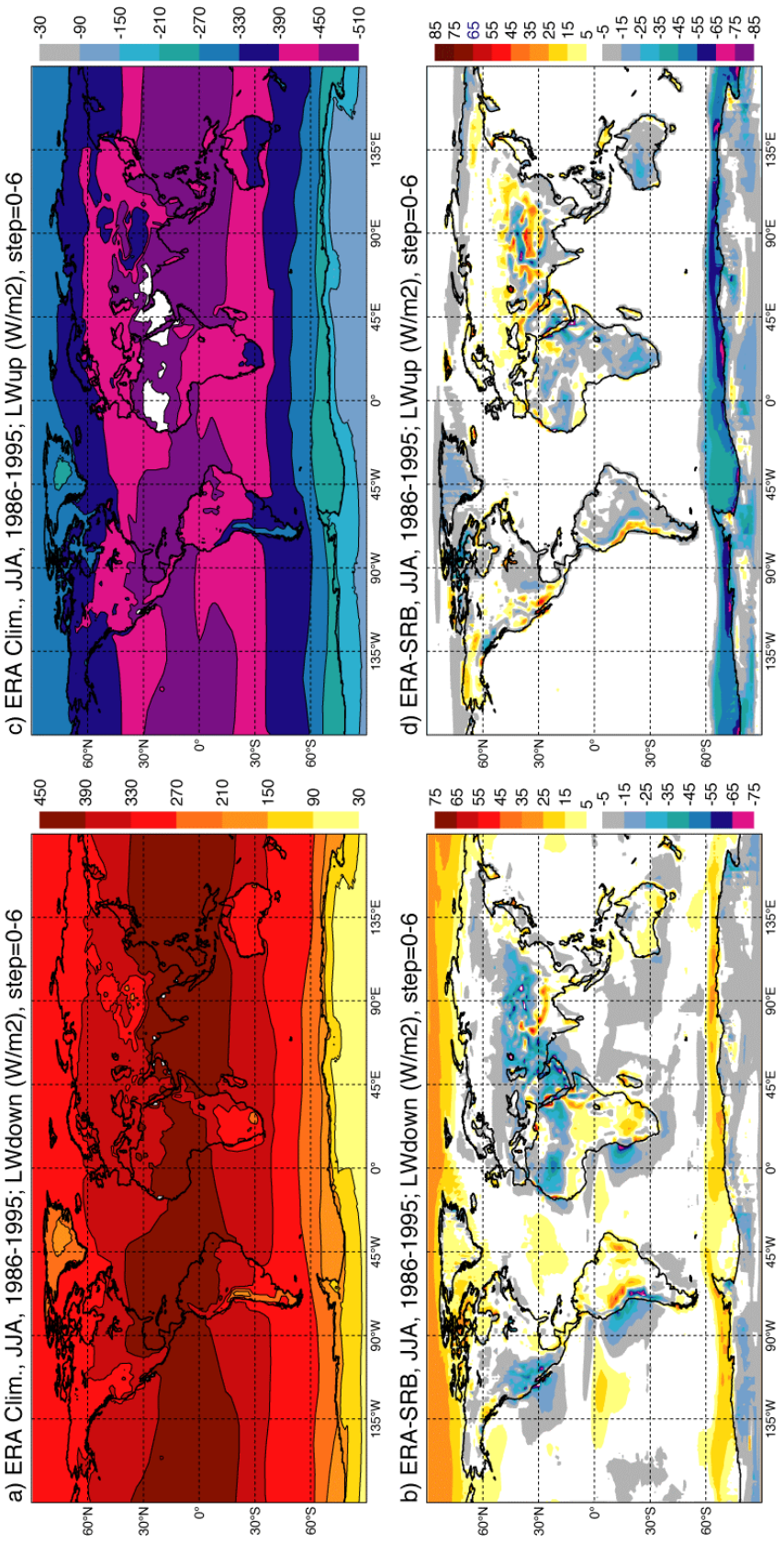

Figure 12: AsFigure 11 for the northern summer, JJA.

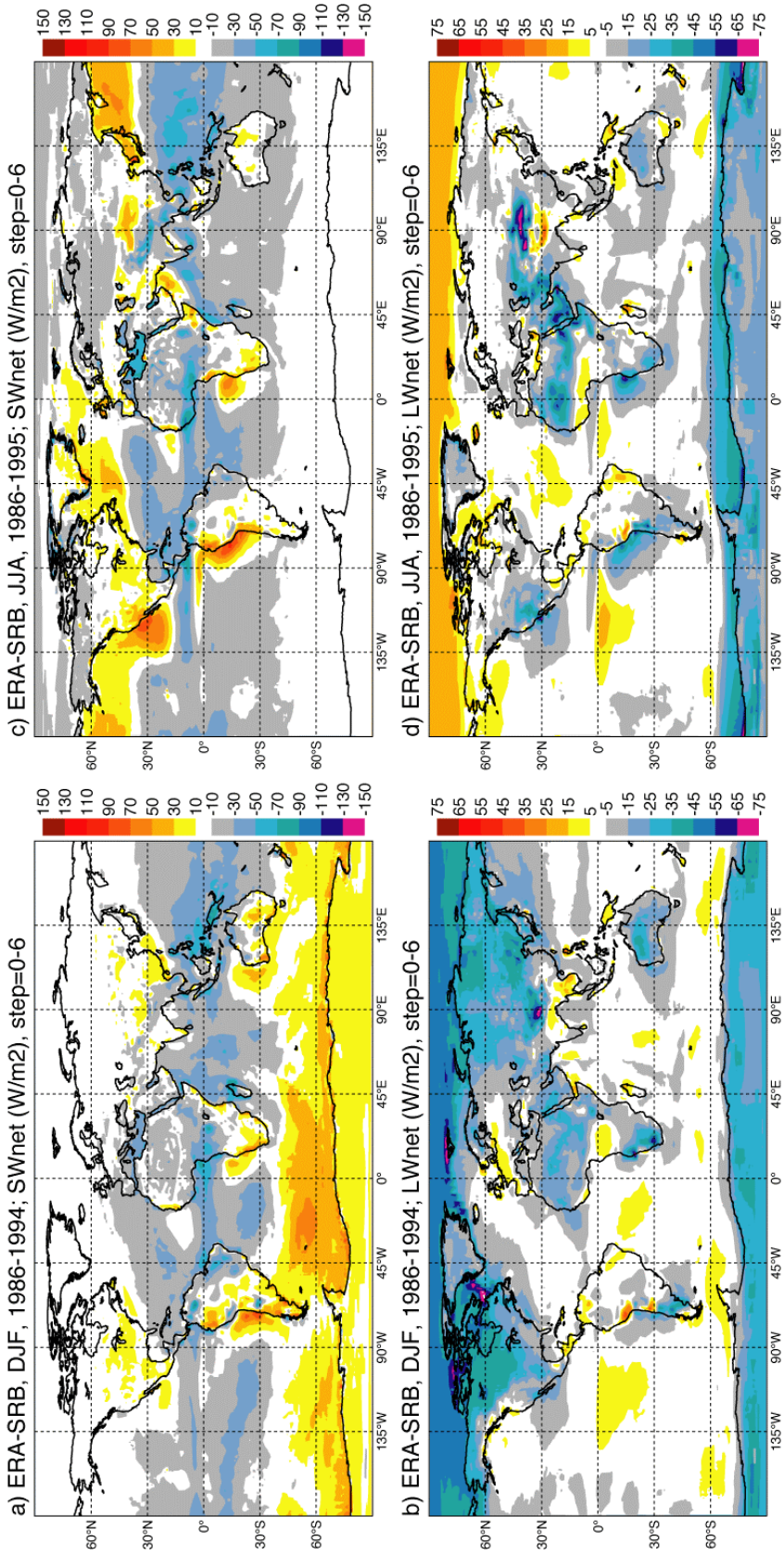

Figure 13: Difference ERA-SRB for SWnet and LWnet for DJF and JJA.

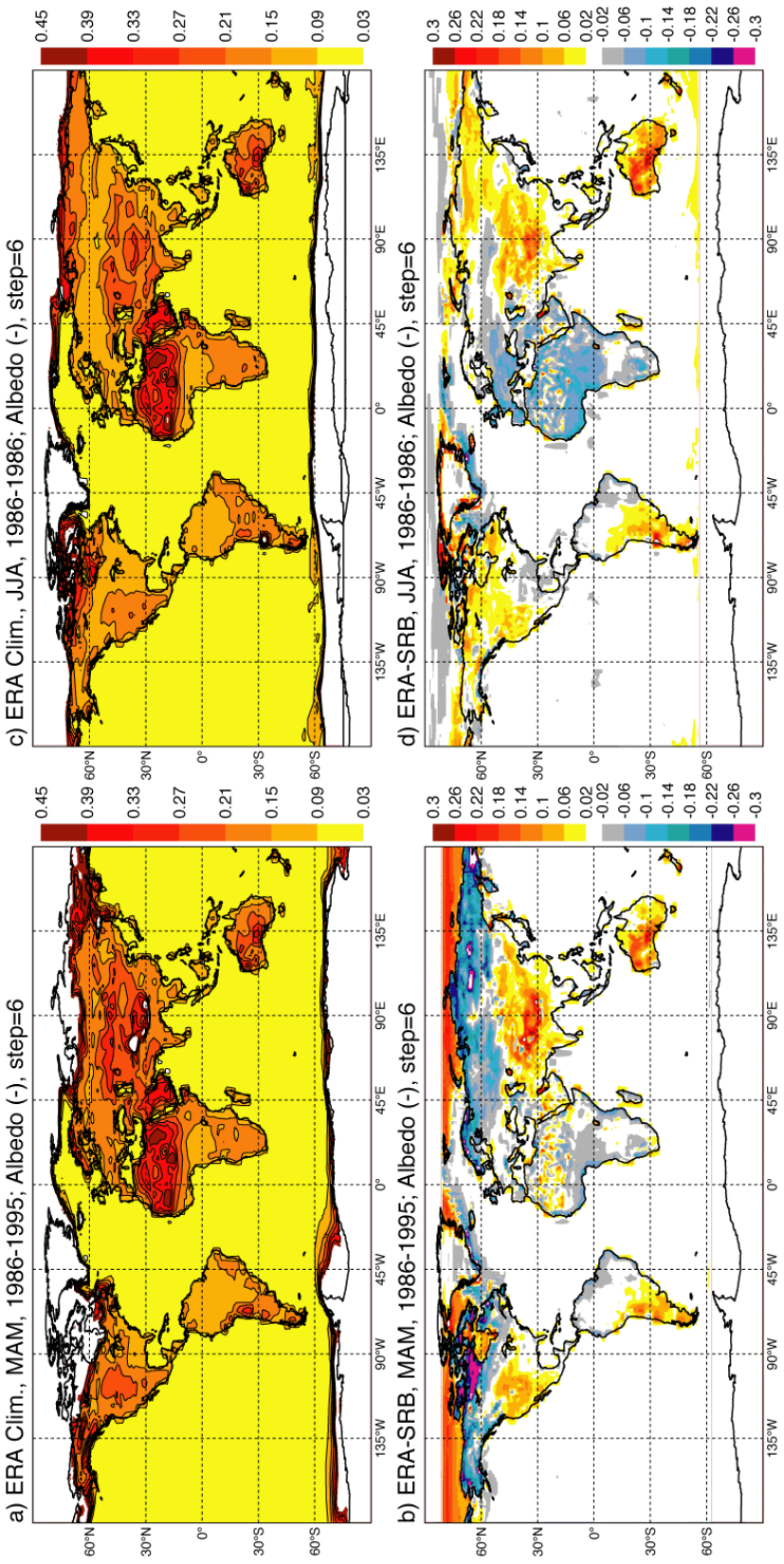

Figure 14: ERA-40 surface all-sky albedo for northern Spring (MAM) and summer JJA (upper) and the difference from the SRB albedo (lower).

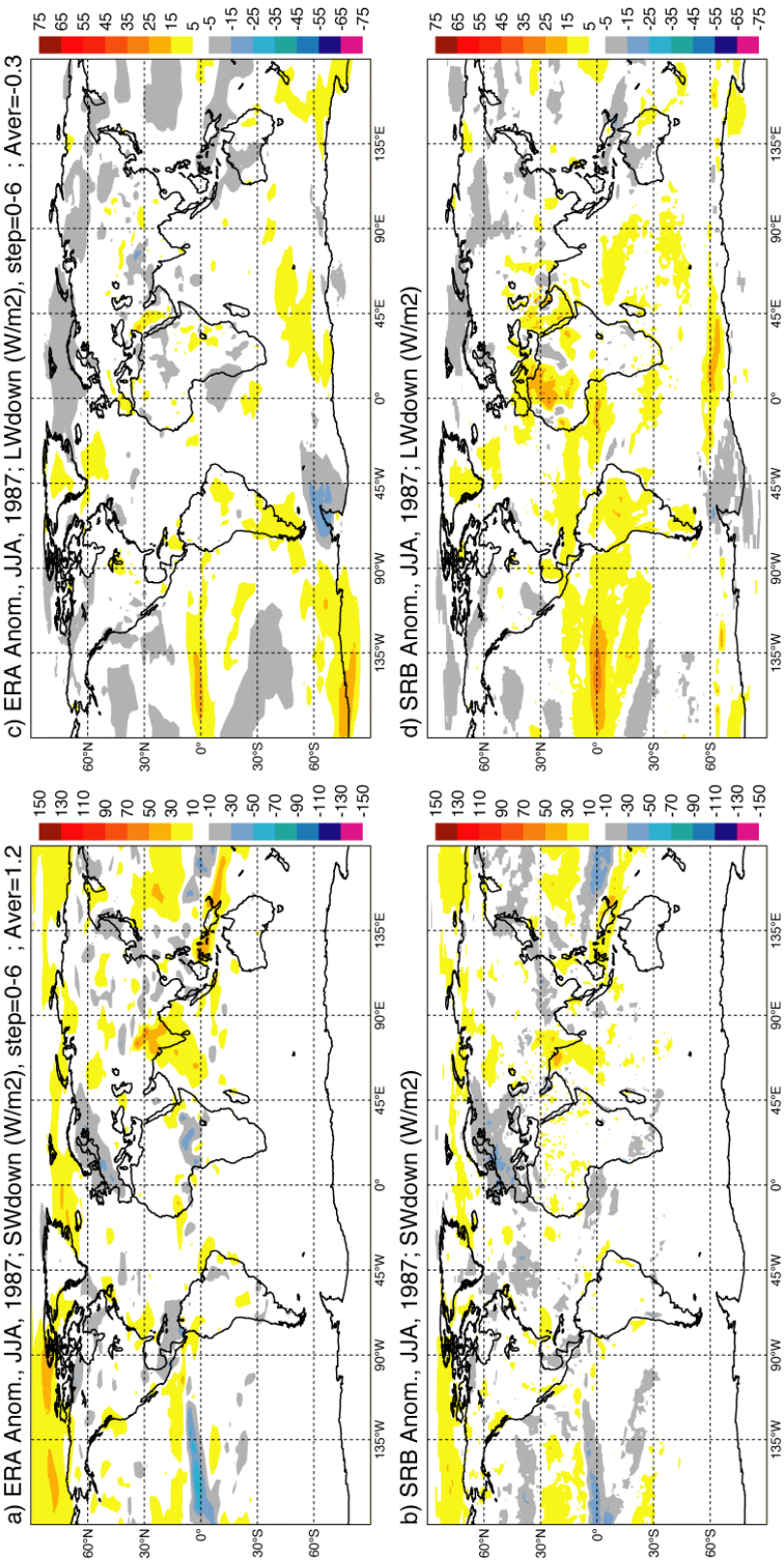

Figure 15: Comparison of ERA-40 and SRB anomalies in SWdown and LWdown for JJA1987.

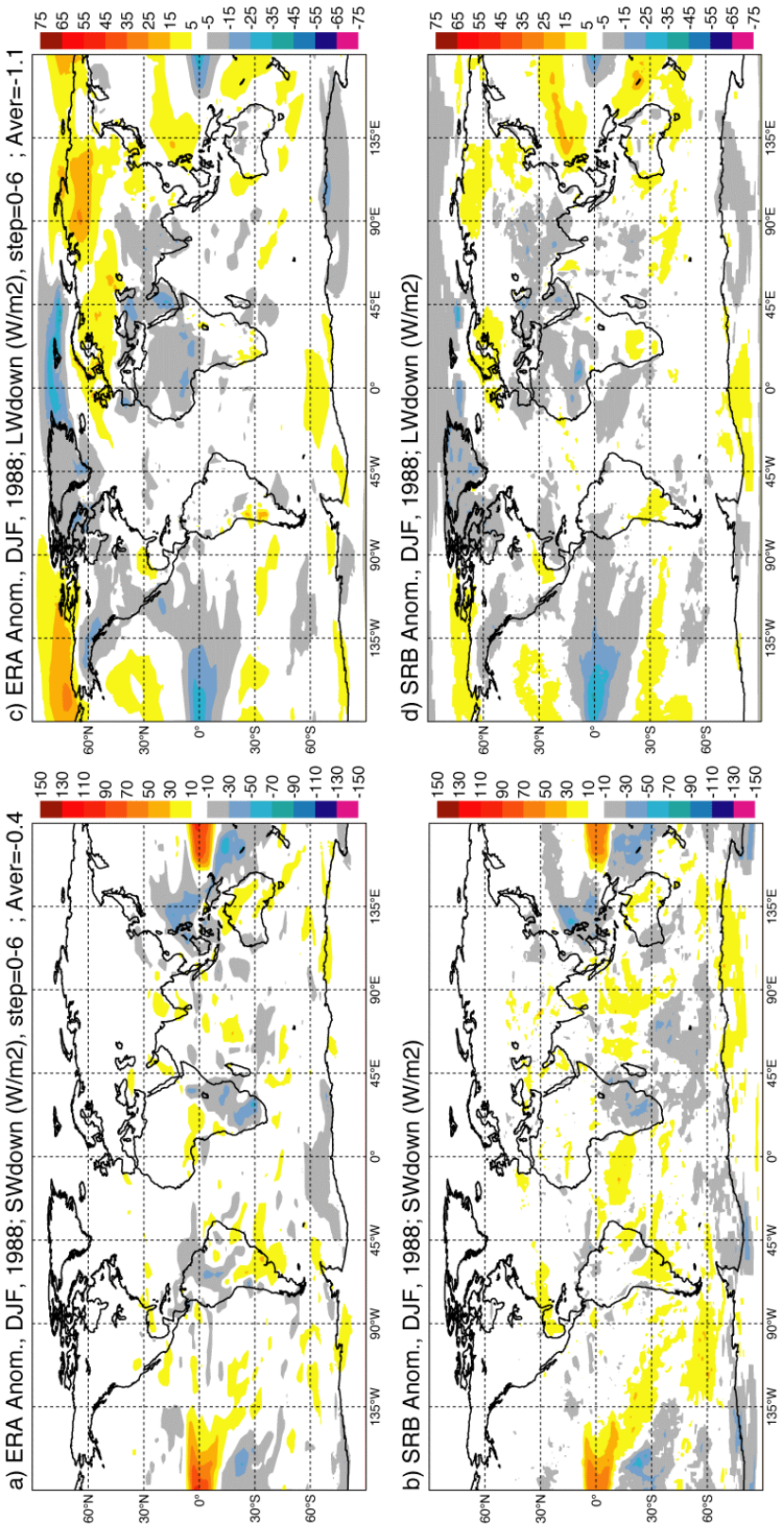

Figure 16: As Figure 15 for DJF 1988.